Available online at www.sciencedirect.com
SCIENCE DIRECT
Polymer 46 (2005) 4899–4908
polymer
www.elsevier.com/locate/polymer

Anisotropic thermal expansion in polypropylene/poly(ethylene-*co*-octene) binary blends: influence of arrays of elastomer domains

Michio Ono[a,b,*], Junichiro Washiyama[a], Ken Nakajima[b], Toshio Nishi[b]

[a]*SunAllomer Ltd, Kawasaki Development Center, 2-3-2 Yako-cho, Kawasaki-ku, Kaswasaki, Kanagawa 210-0863, Japan*
[b]*Department of Organic and Polymeric Materials, Faculty of Engineering, Tokyo Institute of Technology, 1-12-1 Ookayama, Meguro-ku, Tokyo 152-8552, Japan*

Received 22 July 2004; accepted 11 March 2005

Abstract

In injection molded specimens consisting of isotactic polypropylene (iPP)/poly(ethylene-*co*-octene) (EOR) blends with different viscosity ratio of η(EOR)/η(iPP), the coefficient of linear thermal expansion (CLTE) was investigated by thermal mechanical analysis (TMA). It was found that the blend with a smaller viscosity ratio showed the larger anisotropy of CLTE depending upon the directions. TEM observations revealed that the shape of rubber domains varied from slabs, cylinders to ellipsoids in shape, by increasing η(EOR)/η(iPP). The crystal orientation analysis by WAXD have revealed that the blend with 'slab' EOR domains showed the orientation of the *c*-axis of iPP crystals was preferably oriented to FD (flow direction) and TD (transverse to FD), and that the *b*-axis was exclusively oriented to ND (thickness direction). The CLTE of each FD and TD was in good agreement with the rules-of-mixing for CLTE by introducing the effect of the arrays of the elastomer domains and the PP crystal orientation. On the other hand, the CLTE in ND showed massive discrepancy between the calculation and observation. It was found that the incorporation of the retraction effect could explain the discrepancy to some extent.
© 2005 Elsevier Ltd. All rights reserved.

Keywords: Polypropylene; Coefficient of linear thermal expansion; Injection-molding

1. Introduction

Among thermoplastics, isotactic polypropylene (iPP) is outstanding due to its attractive price/performance balance, mechanical properties, processability, and wetherability [1]. Hence, iPP and its alloys (elastomer added) and composites (filled) are widely used in molded articles. They are used as automotive, electric appliance, food packaging, films, sheet and textile fibers processed by injection-, blow molding, extrusion- and spinning.

In automobile applications, it is a common way to incorporate inorganic fillers into PP in order to improve the mechanical properties and dimensional stability. However, the recent demand towards weight reduction and no-ash after combustion has been increasing the use of filler-less PP rather than the filler-reinforced one.

One of the drawbacks of the filler-less PP is the large variation of shrinkage due to temperature change. In fact, the dimensional mismatch between PP resin parts and metals or other plastics parts has been a critical issue; the large discrepancy in the coefficient of linear thermal expansion (CLTE) between the PP ($\sim 10^{-4}$ m/m °C) [2], and metals ($\sim 10^{-5}$ m/m °C) [3] would be the principal cause.

In the case of injection-molded PP articles, deformations so-called 'warpage' occasionally happen. According to Kikuchi and Koyama, the warpage closely related with a ratio (R_α) of the CLTE in the flow direction to that transverse to the flow. They pointed out that R_α was an important parameter for controlling warpage [4].

Despite the practical importance of CLTE in PP, a few systematic studies were performed [5–12]. In particular, only limited attempts have been made to lower CLTE in non-filled PP system [10–12]. Nomura et al. [6] pointed out in PP/EPR/talc system that the retraction force of EPR domains contributed to the reduction in CLTE in FD, and

* Corresponding author. Address: SunAllomer Ltd., Kawasaki Development Center, 2-3-2 Yako-cho, Kawasaki-ku, Kawasaki 210-0863, Japan. Tel.: +81 44 276 3569; fax: +81 44 266 9432.
E-mail address: michio_ono@sunallomer.co.jp (M. Ono).

0032-3861/$ - see front matter © 2005 Elsevier Ltd. All rights reserved.
doi:10.1016/j.polymer.2005.03.098

hence would increase the CLTE in ND. They also pointed out that the PP crystal orientation was important to control CLTE. Recently Wu et al. reported that the injection-molded specimen with iPP/EPR blend systems showed quite large anisotropy in CLTE [11]; note that no talc was added. They suggested that the driving force on the anisotropy was assigned to be the thermal deformation of EPR domains forming co-continuous micro-layers in iPP near the skin portion of specimens. The authors reported in the previous paper [12] that similar anisotropy in CLTE was observed in the iPP/EOR blend systems. The conceivable mechanisms for the anisotropy were pointed out to be the morphology effect of elastomer domains and the PP crystal orientation as similar to Nomura et al. The present paper focused on the influence of morphology of elastomer domains, PP crystal orientation and retraction effect on the anisotropy in the CLTE.

2. Experimental

2.1. Materials

Isotactic polypropylenes (iPP) and ethylene-*co*-octene copolymer rubber (EOR) used in this study were from SunAllomer Ltd, and from Dupont–Dow Elastomer Japan Ltd, respectively. The structural and rheological properties are listed in Table 1. The melt viscosity at 100 s^{-1} (210 °C) of each raw material was determined with a capillary rheometer (Capirograph 1C; Toyo Seiki) using an orifice having $L/D=40$. This shear rate corresponded to that applied upon injection molding [13].

Three binary blends, PP-1/EOR, PP-2/EOR and PP-3/EOR, consisting of 70/30 of iPP/EOR (vol/vol) were prepared by using a co-rotating twin-screw extruder (KTX-30; Kobe Steel) at 160 °C. The characterization of the blends was summarized in Table 2.

Each blend was injection-molded to obtain a slab (125 mm (length)×20 mm (width)×3.0 mm (thickness)) using an injection molding machine (Fanuc α100C; Fanuc) at 200 °C. The injection rate, injection time to full-pack and the tool temperature were 40 mm/s, 2.8 s and 40 °C, respectively.

The crystallinity of the iPP and each blend were determined using the heat of fusion per gram divided by that of perfect crystalline iPP, 209 J/g [14]. The heat of fusion and melting temperatures (T_m) were measured with a differential scanning calorimeter (DSC) (DSC-7; Perkin Elmer) at a scanning rate of 10 °C/min.

2.2. Coefficient of linear thermal expansion (CLTE)

A specimen for the CLTE measurement was cut from the central part of the slab; the size of the specimen was 3.0 mm (height), 5.0 mm (length) and 3.0 mm (width); note that the cross-section was 3.0×5.0 mm^2 in all cases. It should be pointed out that the term 'linear' implied the one-dimensional as commonly used, not linearity; indeed, the non-linear dependence of CLTE on T was reported [11,12]. The specimens were then annealed at 100 °C for 24 h to remove thermal history and residual stress. The measurement was performed in the compression mode using a thermo-mechanical analyzer (TMA) (MTS9000; Shinku Riko) from 23 to 100 °C at a heating rate of 4 °C/min. The applied load was 5.0 g, being sufficient to ensure that the probe remains in contact with the sample and small enough to allow the compression strain to be neglected [12,15]. The CLTE was monitored as a function of temperature in three directions, MD, TD and ND; the definition of FD, TD and ND is shown in Fig. 1. Each measurement was independently made on a different specimen.

The CLTE (αl_J^{obs}) was calculated by Eq. (1)

$$\alpha l_J^{obs} = \frac{1}{L_1}\frac{L_2 - L_1}{T_2 - T_1} \tag{1}$$

where L_1 is the length at T_1 ($T_1=23$ °C in this work) and L_2 is the length at T_2 ($T_2=100$ °C). The subscript J means the directions, FD, TD and ND.

2.3. Morphology observation

An ultra thin section (thickness; 50–60 nm) was microtomed in *X*-, *Y*- and *Z*-faces (shown in Fig. 1) at −100 °C; the thin section was obtained form the core layer for each specimen after being stained in RuO_4 aqueous solution (0.5 wt%) at room temperature for over 24 h. The morphology was observed by transmission electron microscopy (TEM) (JEM1200EX; JEOL) operated at 120 kV.

Table 1
Characteristics of raw materials

Sample designation	Types of polymers	MFR (dg/min)	Flexural modulus (MPa)	T_m (°C)	Crystallinity (%)	Viscosity at 100 s^{-1} (Pa s)
PP-1	Isotactic PP	2.5	1650	166	47	652
PP-2	Isotactic PP	70	1700	165	53	160
PP-3	Isotactic PP	800	1770	162	49	45
EOR	Poly(ethylene-*co*-octene)	10	20	55	n.d.[a]	649

[a] Neligibly small.

Table 2
Characteristics of blend samples

Sample designation	Viscosity ratio at 100 s^{-1}	T_m (°C)
PP-1/EOR	1.0	164
PP-2/EOR	4.0	165
PP-3/EOR	14	161

2.4. PP crystal orientation by WAXD

Wide angle X-ray diffractometer with a pole figure attachment (WAXD)(RAD-3X; Rigaku) using Ni-filtered Cu K_α radiation ($\lambda = 1.5418$ Å) operated at 40 mA and 40 kV was used to investigate the crystalline orientation of PP. The reference axis was chosen to the FD. The samples were sliced to 1 mm thickness by removing skin layers and mounted on a sample holder so that the FD in the sample coincide with the vertical axis in the pole figure. Accordingly, the TD and ND in the sample coincide with transverse- and normal-direction in the pole figure, respectively. Two angle scannings, polar angle (α), and azimuthal angle (β), were made. The transmission mode scanning was made with the α ranging from 0 to 40° and the β ranging from 0 to 360°, and the scans in the reflection mode were carried out with the α from 40 to 90° and the β from 0 to 360°. The angular step of 5° was performed or α and the β scanning was made at a scan speed of 180° or both diffraction modes.

The mean square cosine $\langle\cos^2_{\phi_{c,J}}\rangle$, $\langle\cos^2_{\phi_{a,J}}\rangle$ and $\langle\cos^2_{\phi_{b,J}}\rangle$ which were evaluated using the diffraction from (040) ($2\theta = 16.9°$) and (110) ($2\theta = 14.1°$) planes, where $\phi_{040,J}$ (or $\phi_{110,J}$) is the angle between the normal of (040) plane (or (110) plane) and J direction [16]. The Herman's orientation function for each a-, b- and c-axis, i.e. f_a, f_b and f_c was then determined by the following equations [17]

$$f_{p,J} = \frac{3\langle\cos^2_{\phi_{p,J}}\rangle - 1}{2} \tag{2}$$

$$f_{p,\mathrm{FD}} + f_{p,\mathrm{TD}} + f_{p,\mathrm{ND}} = 0 \tag{3}$$

where p is the crystallographic axis ($p = a$, b and c).

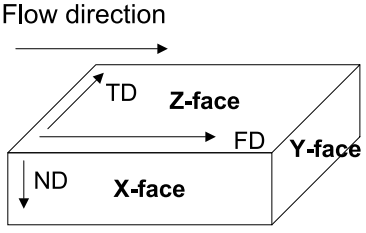

Fig. 1. Definition of the direction, FD for flow direction, TD for transverse-to- flow direction, and ND for normal-to-flow direction as well as the faces, X-face, Y-face, and Z-face.

2.5. CLTE of PP crystal

The lattice spacing as a function of temperature was measured by WAXD equipped with a thermocouple. The measurement was carried out at 23 and 100 °C. The sliced specimen used in the Section 2.4 was mounted on the holder with X-ray exposure parallel to the Z-face, and warmed up to the testing temperature and held at each testing temperature for 10 min prior to X-ray exposure. Using a goniometer, a 2θ scan in the range from 5 to 35° was carried out in the reflection mode at a scan rate of 2°/min.

The α-form PP crystal has a monoclinic crystal structure and showed five strongest reflections 110, 040, 130, 111 and 131 in the WAXD measurement. The lattice constants, a, b, c, and β were determined.

The CLTE (αl_X^{cr}) of the lattice constant was defined viz Eq. (4)

$$\alpha l_X^{\mathrm{cr}} = \frac{1}{X_1}\frac{X_2 - X_1}{T_2 - T_1} \tag{4}$$

where X denoted lattice constant a, b and c, X_1 and X_2 denoted the lattice constant at T_1 ($T_1 = 23$ °C in this work) and T_2 ($T_2 = 100$ °C), respectively.

3. Results and discussion

3.1. Influence of viscosity ratio on CLTE

Fig. 2 showed the CLTE's in the FD, TD and ND directions (designated as $\alpha l_{\mathrm{FD}}^{\mathrm{obs}}$, $\alpha l_{\mathrm{TD}}^{\mathrm{obs}}$ and $\alpha l_{\mathrm{ND}}^{\mathrm{obs}}$) as a function of a viscosity ratio of EOR to iPP, η(EOR)/η(iPP). It was found that the $\alpha l_{\mathrm{FD}}^{\mathrm{obs}}$ and $\alpha l_{\mathrm{TD}}^{\mathrm{obs}}$ increased, while the $\alpha l_{\mathrm{ND}}^{\mathrm{obs}}$

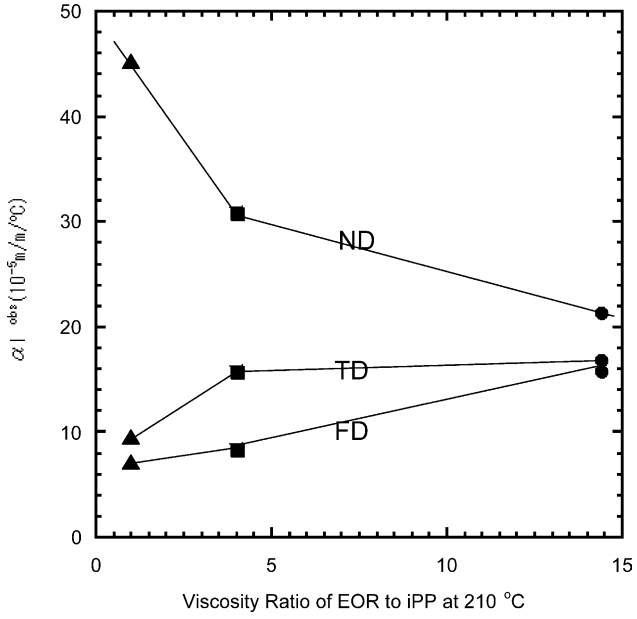

Fig. 2. CLTE as a function of viscosity ratio of η(EOR) to η(iPP); (▲) PP-1/EOR, (■) PP-2/EOR, and (●) PP-3/EOR.

decreased, when the viscosity ratio increased. In addition, the anisotropy became stronger when the viscosity ratio was smaller as demonstrated in the PP-1/EOR system.

The volumetric thermal expansion (CVTE) obtained by the summation of αl_{FD}^{obs}, αl_{TD}^{obs} and αl_{ND}^{obs} was 63, 55 and 54 (10^{-5}/°C) for PP-1/EOR, PP-2/EOR and PP-3/EOR, respectively. It should be pointed out that small difference in the CVTE among PP-1/EOR, PP-2/EOR and PP-3/EOR was found despite the massive difference in the CLTE in the FD, TD and ND. Wu et al. also reported the variation in CVTE to be small even when anisotropy was large [11]. The present observation was thus in accordance with the results by Wu et al.

3.2. Morphology observation by TEM

3.2.1. PP-1/EOR

Fig. 3(a) and (b) showed TEM micrographs at low magnification of *X*- and *Y*-face for PP-1/EOR, respectively. The dark and bright phases indicated EOR-rich and iPP-rich phases, respectively. From these observations, the shape of the EOR domains would be a slab as observed in the previous study [12].

Fig. 3(c) and (d) showed TEM micrographs at higher magnification of *X*-, and *Y*-face for PP-1/EOR, respectively. The PP crystal was found to be oriented normal to the EOR slab as observed in Fig. 3(c) and (d). Fig. 3(e) showed the rectangular structure. These observations suggested that epitaxial growth of PP crystals on the EOR slab. Such a pillar structure was also reported in PP/EPR/talc systems [5,6]. The PP crystal orientation in the PP-1/EOR system would thus be strong.

3.2.2. PP-2/EOR

Fig. 4(a) and (b) showed TEM micrographs of *X*- and

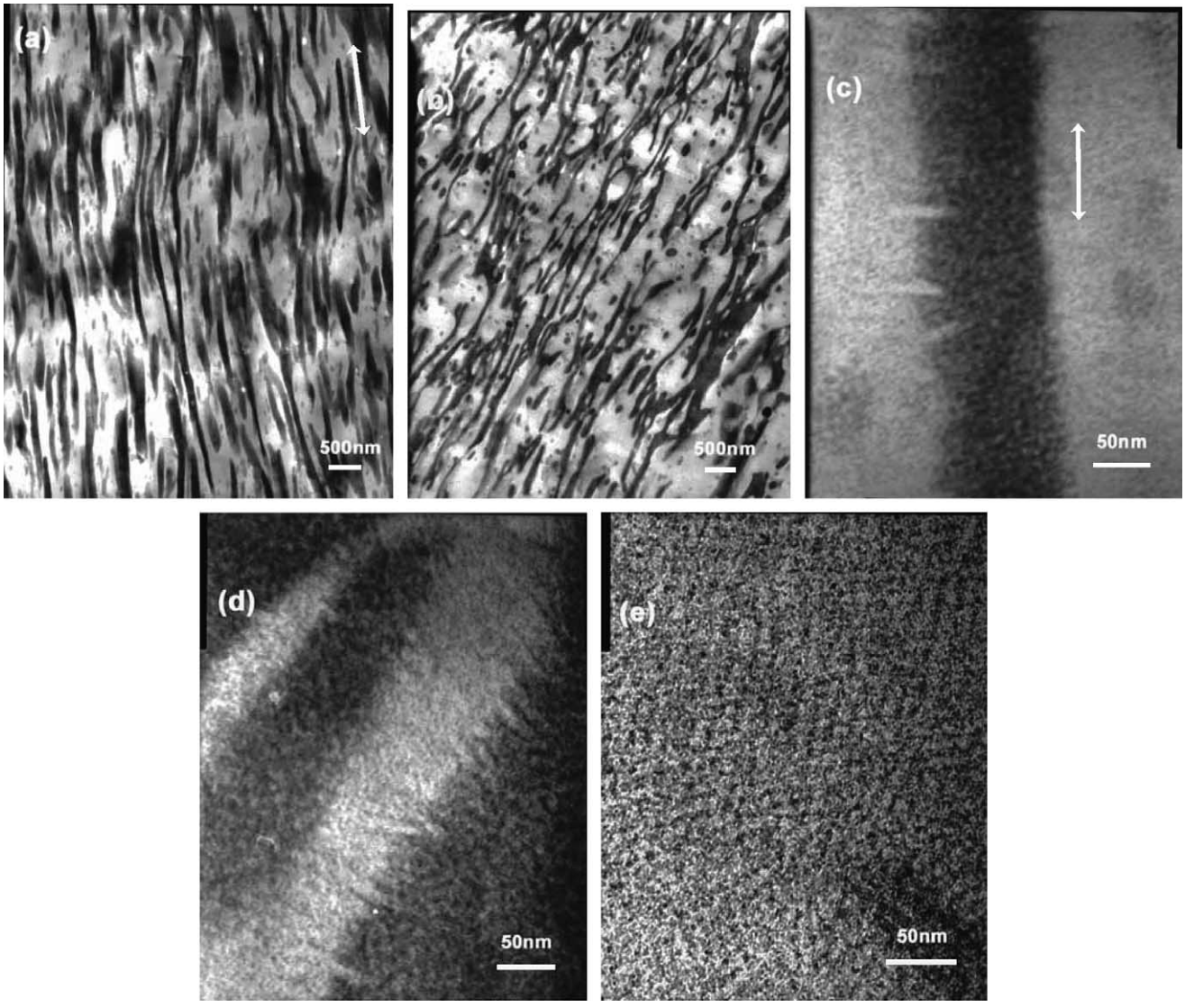

Fig. 3. TEM micrographs of PP-1/EOR (a) from *X*-face, (b) from *Y*-face, (c) from *X*-face at high magnification, (d) from *Y*-face at high magnification and (e) from *Z*-face at high magnification.

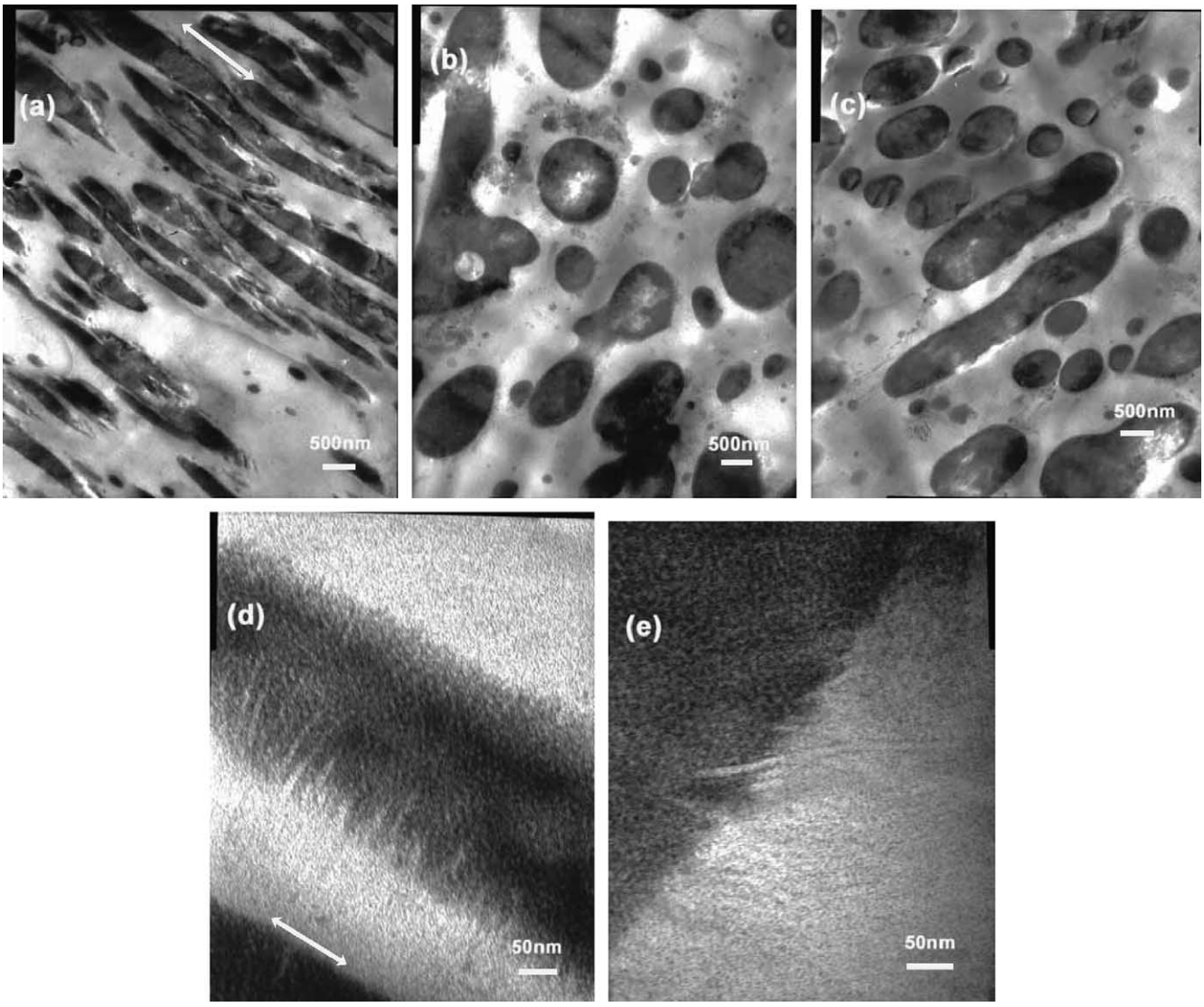

Fig. 4. TEM micrographs of PP-2/EOR (a) from *X*-face, (b) from *Y*-face, (c) from *Y*-face at a different portion, (d) at high magnification and (e) from *Y*-face at high magnification.

Y-face for PP-2/EOR, respectively. The image of the EOR domains in *X*- and *Y*-views were found to be needle and circular, respectively, indicating that the shape of the EOR domains would principally be cylindrical. It should be noted that slab-like domains of EOR also observed sporadically as shown in Fig. 4(c) (*Y*-face).

Fig. 4(d) and (e) showed TEM micrographs at higher magnification of *X*- and *Y*-face for PP-2/EOR, respectively. As similar to the PP-1/EOR system, the PP lamellae were found to be oriented normal to the EOR domain in the *X*-face as observed in Fig. 4(d), while in the *Y*-face, the PP lamellae penetrated randomly into EOR domains (Fig. 4(e)). The PP crystal orientation in the PP-2/EOR system would thus be weaker than that in PP-1/EOR system.

3.2.3. PP-3/EOR

Fig. 5(a) and (b) showed TEM micrographs of *X*- and *Y*-face for PP-3/EOR, respectively. The image of the EOR domains in *X*- and *Y*-face views were found to be circular in all directions, indicating that the shape of the EOR domains would be spherical (ellipsoid).

Fig. 5(c) showed TEM micrographs at higher magnification of the *X*-face. As similar to the PP-2/EOR in the *Y*-face, the PP lamellae were found to be penetrated randomly into EOR domains. The PP crystal orientation in the PP-3/EOR system would thus be random.

More detailed study on the PP crystal orientation will be made using X-ray diffraction method in Section 3.3.

3.3. PP crystal orientation

The orientation function f_a, f_b and f_c obtained from the WAXD for each direction were summarized in Table 3. In the case of PP-1/EOR, the f_c was the largest in both FD and

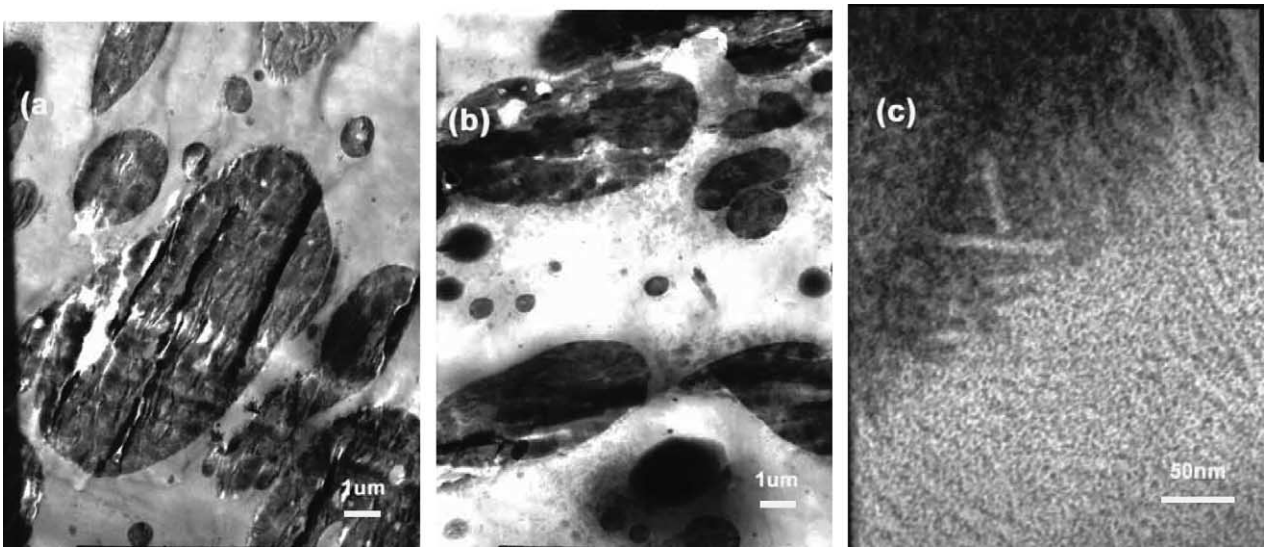

Fig. 5. TEM micrographs of PP-3/EOR (a) from *X*-face, (b) from *Y*-face and (c) from *X*-face at high magnification.

TD, and the f_b was the largest in ND, indicating that *c*-axis was principally oriented to FD and TD, whereas *b*-axis to ND. In the case of PP-2/EOR, similar orientation was found. It should, however, be noted that the f_c in FD for PP-1/EOR was nearly two-fold higher and the f_b in ND for PP-1/EOR was more than three times larger in comparison with those in the PP-2/EOR system. These observations indicated that the *c*- and *b*-axis orientation to FD and ND in PP-1/EOR was much stronger than those in the PP-2/EOR system. In the PP-3/EOR system, the orientation of PP crystals seemed to be relatively weaker in comparison with other two.

It should be pointed out from the X-ray and TEM studies that the PP crystal orientation depended strongly on the morphology (shape) of the elastomer domains in these systems.

3.4. CLTE of lattice constants

The CLTE for the lattice constant (αl_a^{cr}, αl_b^{cr} and αl_c^{cr}) was summarized in Table 4. We obtained from Table 4, $\alpha l_c^{cr} < \alpha l_a^{cr} \ll \alpha l_b^{cr}$ and αl_c^{cr} to be negative. Gu et al. have reported that the thermal expansion of PP crystal along the *b*-axis was 2.6 folds greater than that along the *a*-axis: that along the *c*-axis was ~10% of the *a*-axis [18]. The present results were thus in consistent with Gu et al. It should be pointed out that each lattice constant for PP-1 and the three blends was found to be equal, indicating that the presence of elastomers and their arrays had no influence of the CLTE of PP crystal.

We estimated the anisotropy of the CLTE in the PP phase by taking account the anisotropy in the CLTE and orientation of PP crystals. Applying the series model PP between crystal and amorphous phases in PP, the CLTE of PP was given by Eq. (5) [19]

$$\alpha l_J^{PP-X} = (1-c)\alpha l^{am} + c\alpha l_J^{cr} \quad (5)$$

where *c*, αl^{am} and αl^{cr} denoted crystallinity, CLTE of PP amorphous part and CLTE of PP crystal part, respectively. The superscript PP-*X* denoted PP-1, PP-2 and PP-3, and the subscript *J* represented FD, TD and ND as defined in Fig. 1. The αl_J^{cr} in Eq. (5) was given by $f_a^J \alpha l_a + f_b^J, \alpha l_b + f_c^J, \alpha l_c$. Finally we obtained Eq. (6) for the CLTE of PP for each direction *J* (=FD, TD and ND)

$$\alpha l_J^{PP-X} = (1-c)\alpha l^{am} + c(f_a^J \alpha l_a + f_b^J \alpha l_b + f_c^J \alpha l_c) \quad (6)$$

Here, the αl^{am} was assumed to be isotropic and, hence, being one third of the coefficient volume thermal expansion (αl^{am}=23 (10^{-5} m/m/°C)) [20]. Note that anisotropy in the

Table 3
Orientation function of PP crystalline part in the blend

Sample designation	Orientation function	Direction		
		FD	TD	ND
PP-1/EOR	f_a	0.0090	−0.029	0.012
	f_b	−0.24	−0.082	0.26
	f_c	0.23	0.11	−0.28
PP-2/EOR	f_a	0.010	−0.064	0.0050
	f_b	−0.13	−0.021	0.081
	f_c	0.12	0.085	−0.086
PP-3/EOR	f_a	−0.023	0.028	−0.077
	f_b	0.096	−0.084	−0.022
	f_c	−0.073	0.056	0.099

Table 4
CLTE for lattice constants of PP crystalline part in the blend from 23 to 100 °C

Sample designation	Viscosity ratio at 100^{s-1}	CLTE (10^{-5} m/m/°C)		
		αl_a^{cr}	αl_b^{cr}	αl_c^{cr}
PP-1	–	8.2	18	−0.41
PP-1/EOR	1.0	8.8	19	−1.2
PP-2/EOR	4.0	8.2	18	−0.85
PP-3/EOR	14	9.1	17	−0.40

amorphous phase would not be critical because the *c*-axis showed orientation along FD rather than ND (our focus). Indeed, Choy et al. [8] treated the amorphous phase to be isotropic.

3.5. CLTE modeling

There were a number of theoretical studies on the CLTE for filler reinforced plastics [21–28]. These investigations have revealed that the CLTE anisotropy greatly depended upon the shapes, arrays or directions of filler inclusions. In the present case, the elastomer domains corresponded to the filler inclusions. In addition, the effect of morphology and anisotropy in PP crystal (in CLTE) could be incorporated to the model.

Prior to the CLTE modeling, the following assumptions were made; (1) consisting of two components, PP and EOR, (2) perfect adhesion between PP and EOR.

Taking account into the anisotropy effect of PP, we derived the formulae of CLTE for PP-1/EOR (slab), PP-2/EOR (cylindrical) and PP-3/EOR (spherical). As discussed in Appendix A, the anisotropic effect of elastic constants would be negligible, so that we assumed the elastic constant to be isotropic.

3.5.1. PP-1/EOR with slab elastomer phase

In this case, the elastomers aligned parallel to both in FD and TD and in series in ND. The thermal stress, $\sigma(=\alpha l\Delta \mathrm{TE})$ developed in FD and TD was thus the summation of a thermal stress for each component. As for ND, a thermal strain, $\varepsilon(=\alpha l\Delta T)$ in ND was the summation of a thermal strain for each component [28]. The final formula of CLTE for each direction was given by Eqs. (7)–(9)

$$\alpha l_{\mathrm{FD}}^{\mathrm{PP}-1}(\mathrm{calc}) = \frac{\alpha l_{\mathrm{FD}}^{\mathrm{PP}-1}\phi^{\mathrm{PP}-1} + \alpha l^{\mathrm{EOR}}\xi\phi^{\mathrm{EOR}}}{\phi^{\mathrm{PP}-1} + \xi\phi^{\mathrm{EOR}}} \tag{7}$$

$$\alpha l_{\mathrm{TD}}^{\mathrm{PP}-1}(\mathrm{calc}) = \frac{\alpha l_{\mathrm{TD}}^{\mathrm{PP}-1}\phi^{\mathrm{PP}-1} + \alpha l^{\mathrm{EOR}}\xi\phi^{\mathrm{EOR}}}{\phi^{\mathrm{PP}-1} + \xi\phi^{\mathrm{EOR}}} \tag{8}$$

$$\alpha l_{\mathrm{ND}}^{\mathrm{PP}-1}(\mathrm{calc}) = \alpha l_{\mathrm{ND}}^{\mathrm{PP}-1}\phi^{\mathrm{PP}-1} + \alpha l^{\mathrm{EOR}}\phi^{\mathrm{EOR}} \tag{9}$$

where $\xi = E^{\mathrm{EOR}}/E^{\mathrm{PP}-1}$.

3.5.2. PP-2/EOR with cylindrical elastomer phase

The CLTE model for fiber-reinforced plastics was applicable to this system. The model by Shapery [25] was the most suitable for the present case. This model assumed that the complementary energy accompanying by a thermal stress was equal to the Gibbs's free energy of the entire body. The calculated CLTE were then given by Eqs. (10)–(12).

$$\alpha l_{\mathrm{MD}}^{\mathrm{PP}-2}(\mathrm{calc}) = \frac{\alpha l_{\mathrm{FD}}^{\mathrm{PP}-2}\phi^{\mathrm{PP}-2} + \alpha l^{\mathrm{EOR}}\xi\phi^{\mathrm{EOR}}}{\phi^{\mathrm{PP}-2} + \xi\phi^{\mathrm{EOR}}} \tag{10}$$

$$\begin{aligned}\alpha l_{\mathrm{TD}}^{\mathrm{PP}-2}(\mathrm{calc}) = {} & (1+\nu^{\mathrm{PP}-2})\alpha l_{\mathrm{TD}}^{\mathrm{PP}-2}\phi^{\mathrm{PP}-2} \\ & +(1+\nu^{\mathrm{EOR}})\alpha l^{\mathrm{EOR}}\phi^{\mathrm{EOR}} \\ & -(\nu^{\mathrm{PP}-2}\phi^{\mathrm{PP}-2}+\nu^{\mathrm{EOR}}\phi^{\mathrm{EOR}})\alpha l_{\mathrm{FD}}^{\mathrm{PP}-2}\end{aligned} \tag{11}$$

$$\begin{aligned}\alpha l_{\mathrm{ND}}^{\mathrm{PP}-2}(\mathrm{calc}) = {} & (1+\nu^{\mathrm{PP}-2})\alpha l_{\mathrm{ND}}^{\mathrm{PP}-2}\phi^{\mathrm{PP}-2} \\ & +(1+\nu^{\mathrm{EOR}})\alpha l^{\mathrm{EOR}}\phi^{\mathrm{EOR}} \\ & -(\nu^{\mathrm{PP}-2}\phi^{\mathrm{PP}-2}+\nu^{\mathrm{EOR}}\phi^{\mathrm{EOR}})\alpha l_{\mathrm{FD}}^{\mathrm{PP}-2}\end{aligned} \tag{12}$$

where $\xi = E^{\mathrm{EOR}}/E^{\mathrm{PP}-2}$.

3.5.3. PP-3/EOR with spherical elastomer phase

In this case, the arrangement of elastomers is considered to be isotropic in all directions. Consequently, the model by Wang and Kwei [26] was applied to this case. This model assumed that induced thermal stress at the interface between filler and plastics was limited only to the neighborhood of the interface; CLTE was then given by;

$$\alpha l_{J}^{\mathrm{PP}-3}(\mathrm{calc}) = \alpha l_{J}^{\mathrm{PP}-3}\left[1-\phi^{\mathrm{EOR}}\left(1-\frac{\alpha l^{\mathrm{EOR}}}{\alpha l^{\mathrm{PP}-3}}\right)\theta\right] \tag{13}$$

where

$$\theta = \frac{3\xi(1-\nu^{\mathrm{PP}-3})}{\xi[2\phi^{\mathrm{EOR}}(1-2\nu^{\mathrm{PP}-3})+(1+\nu^{\mathrm{PP}-3})]+2(1-2\nu^{\mathrm{EOR}})(1-\phi^{\mathrm{EOR}})} \tag{14}$$

with $\xi = E^{\mathrm{EOR}}/E^{\mathrm{PP}-3}$.

In these Eqs. (7)–(14), E, ν and ϕ denoted Young's modulus, Poisson's ratio and volume fraction (of each component), respectively.

3.6. Comparison with experiment

In the present case, $\phi^{\mathrm{PP}-1}=\phi^{\mathrm{PP}-2}=\phi^{\mathrm{PP}-3}=0.70$ and $\phi^{\mathrm{EOR}}=0.30$. The Young's modulus of each component, $E^{\mathrm{PP}-1}$, $E^{\mathrm{PP}-2}$, $E^{\mathrm{PP}-3}$ and E^{EOR}, was summarized in Table 1.

The Poisson's ratio ν for PP-1, -2, -3 and EOR were assumed to be $\nu^{\mathrm{PP}-1}=\nu^{\mathrm{PP}-2}=\nu^{\mathrm{PP}-3}=0.4$ and $\nu^{\mathrm{EOR}}=0.50$. The αl^{EOR} is 19 (10^{-5} m/m/°C) as one third of the measured CVTE determined with pressure–volume–temperature (PVT) analysis [12]. Moreover, the anisotropy in the CLTE of EOR in the blend was negligibly small because the each CLTE for FD, TD and ND in injection-molded specimen with pure EOR showed almost identical value [12]. Substituting the necessary values summarized in Table 1–4 into Eqs. (6)–(14), we estimated the CLTE of the blends. The results were summarized in Table 5 and compared with the observed results.

It was found form Table 5 that the calculated CLTEs were in good agreement with the observed one except for those in ND for PP-1/EOR and PP-2/EOR. The authors have

Table 5
Calculated CLTE with the effect of arrays of elastomers and PP crystalline orientation taken into consideration

Sample designation	αl_{FD}		αl_{TD}		αl_{ND}	
	Calc	Obs.	Calc	Obs.	Calc	Obs.
PP-1/EOR	10	7.2	11	10	19	45
PP-2/EOR	10	8.3	15	16	16	31
PP-3/EOR	17	16	16	17	16	21

pointed out in a previous study that a simple composite model (slab morphology), which incorporated no anisotropy in PP phase, was not able to account for the massive anisotropy of CLTE between FD and ND; in PP-1/EOR, $\alpha l_{ND}/\alpha l_{FD} \sim 1.2$ (calc) and ~ 6.3 (obs.). In the present model, discrepancy was improved to some extent; $\alpha l_{ND}/\alpha l_{FD} \sim 1.9$ (calc) and ~ 6.3 (obs.), although massive discrepancy could still be found. In addition, similar discrepancy was observed in PP-2/EOR; $\alpha l_{ND}/\alpha l_{FD} \sim 1.6$ (calc) and ~ 3.7 (obs.).

According to Wu et al. [11], the contribution of the micro-layer forming co-continuous phase near the skin layer was important; the contribution would be given by Eq. (15)

$$\alpha l_{ND}/\alpha l_{FD} \sim 1 + 3\psi(1 + \alpha l^{EOR} l/\alpha l^{PP}) \quad (15)$$

where ψ denoted the skin layer fraction. Inserting $\alpha l^{EOR} l/\alpha l^{PP} \sim 2$ and $\psi = L_{skin}/L_0 \sim 1/10$, we would thus obtain $\alpha l_{ND}/\alpha l_{FD} \sim 1.9$. Thus, the micro-layer deformation model would account for some portion of the anisotropy. The ψ increased with decreasing the thickness of the specimen, thus thinner specimen would result in a larger $\alpha l_{ND}/\alpha l_{FD}$ as mentioned in the study [11].

3.7. Retraction effect

Neither orientation of PP crystal model or the micro-layer deformation model could account fully for the massive discrepancy of CLTE in FD and ND; $\alpha l_{ND}/\alpha l_{FD} \sim 6$. In this section, the effect of retraction in elastomer domains was discussed.

As derived in Appendix B, the deformation by retraction force along ND was estimated by Eq. (16)

$$\frac{\Delta L_{ND}}{L_{ND}} \approx \frac{n*}{L_{ND}} \frac{8\gamma}{E} \frac{t}{x} \quad (16)$$

where n^*/L_{ND} and γ denoted the number of slab per unit length and interfacial tension between PP and EOR. t and x were given in Fig. 6.

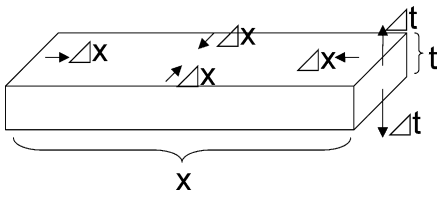

Fig. 6. Deformation mode by retraction.

From the TEM observation in Fig. 3(a), n^*/L_{ND} and t/x were estimated to be $\sim 6 \times 10^6$ and $\sim 10^{-2}$, respectively. In addition, we obtained $E^{EOR} \sim 5 \times 10^4$ (Pa) and $\gamma \sim 1.2 \times 10^{-3}$ (J/m^2) (measured). Inserting these numbers into Eq. (16), we obtained $\Delta L_{ND}/L_{ND} \sim 12 \times 10^{-3}$. This contribution to the αl_{ND} was thus given by $\Delta L_{ND}/(\Delta T \times L_{ND})$. Inserting $\Delta T = 77$ °C, we obtained $\Delta L_{ND}/(\Delta T \times L_{ND})$ to be ~ 15 (10^{-5} m/m/°C). Combining the contribution from retraction with that from the anisotropy by the PP crystal orientation, we obtained $\alpha l_{ND} \sim 34$ (10^{-5} m/m/°C), and hence, $\alpha l_{ND}/\alpha l_{FD} \sim 3.4$, being closer to the observation. Hence, the deformation arising from the retraction in ND would be effective to αl_{ND} [30].

For more precise estimation, however, detailed knowledge on the morphology, elastic constant at an elevated temperature as well as the more refined formulation of the Eq. (16) would be necessary. In the case of PP-2/EOR, the existence of slab-shape domains (Fig. 4(c)) would also result in a greater number of αl_{ND} as similar to PP-1/EOR. It should be noted that the constraint of the deformation of elastomer in FD and TD would result in a larger αl_{ND} as pointed out by Wu et al. [11]. In this case refinement of the Eqs. (7)–(9) would be required.

4. Conclusions

The coefficient of linear thermal expansion, (CLTE), of a polymer blend consisting of polypropylene (PP) and poly(ethylene-*co*-octene) (EOR) with a different viscosity ratio, η(EOR)/η(iPP), was investigated by TMA. As decreasing η(EOR)/η(iPP), the CLTE depended strongly on the directions, namely, FD, TD and ND. TEM observations revealed that the shape of the EOR domains was 'slab', the normal vector of which was parallel to the ND when η(EOR)/η(iPP) = 1.0, 'cylinder' when η(EOR)/η(iPP) = 4.0 and 'ellipsoid or spherical' η(EOR)/η(iPP) = 14.4. WAXD analysis on the orientation function revealed that PP crystal growth was strongly dependent upon the shape in elastomer domains; the *c*-axis were grown parallel to FD, and the *b*-axis parallel to ND.

Taking account the morphology and anisotropy in CLTE of PP crystals, we estimated the CLTE in FD, TD and ND based on the composite model. It was found that the incorporation of the anisotropy in PP resulted in a better prediction in αl_{ND} in comparison with the model without the

anisotropy in PP. However, substantial difference between the model and observation still remained. The effect of retraction deformation was then estimated. It was found that the effect of the deformation by retraction would be important to explain the larger number of αl_{ND}.

Acknowledgements

The authors would like to thank Dr K. Tagashira and Dr K. Yamada of SunAllomer Ltd for their assistance and fruitful discussion on WAXD.

Appendix A

From Eqs. (7), (8) and (11), the variation of CLTE can be obtained through the Taylor expansion in terms of $\Delta\xi$ to the first order, and given by Eq. (A1), where $X=1$ and 2, and $J=$FD and TD

$$\Delta\ln(\alpha l^{PP-X/EOR}) = \frac{\Delta\alpha l_J^{PP-X/EOR}}{\alpha l_J^{PP-X/EOR}} = \frac{\phi^{EOR}(\alpha l^{EOR} - \alpha l_J^{PP-X})}{\alpha l_J^{PP-X}\phi^{PP-X}}\Delta\xi \quad \text{(A1)}$$

Note that in this calculation, we used $\xi \sim 10^{-2}$ from experimental (small).

Substituting $\phi^{EOR}=0.3$, $\phi^{PP-X}=0.7$, $\alpha l^{EOR}-\alpha l^{PP-X})/\alpha l^{PP-X} \sim 1.3$ and $\Delta\xi$ $(\equiv\Delta[E^{EOR}/E^{PP-X}]) < 20\times10^6\times(1/2\times10^9 - 1/40\times10^9) < 10^{-2}$ [29] at room temperature, we obtain Eq. (A2).

$$\frac{\Delta\alpha l_J^{PP-X/EOR}}{\alpha l_J^{PP-X/EOR}} < 5\times10^{-3} \quad \text{(A2)}$$

At an elevated temperature, $\Delta[E^{EOR}/E^{PP-X}] < 10^6\times(1/200\times10^6 - 1/40\times10^9) < 10^{-2}$ indicating that ξ would be also negligible.

The effect of anisotropy in elastic constant would thus be negligible. Note that in the case of PP-3/EOR system, the PP orientation was found to be almost isotropic. E^{PP-3} can thus be isotropic one.

Appendix B

According to Gramespacher et al. [31], the driving force of the retraction is attributed to the interfacial energy reduction. The free energy variation, ΔG, based on the surface area change, ΔA, is thus given by Eq. (B1), where γ denotes interfacial tension between PP and EOR

$$\Delta G = \gamma\Delta A \quad \text{(B1)}$$

Referring Fig. 6, ΔA is given by Eq. (B2), where $t/x \gg 1$ is used

$$\Delta A = 4(x-t)\Delta x \approx 4x\Delta x \quad \text{(B2)}$$

From the volumetric consideration, we obtain Eq. (B3).

$$\frac{\Delta t}{\Delta x} = -2\frac{t}{x} \quad \text{(B3)}$$

The Eq. (B3) corresponds to the Poisson's ratio, $\nu \equiv -(\Delta x/x)/(\Delta t/t)$, to be 0.5 (no volume change). The retraction force, f_{ret}, and the displacement, Δx, are then given by Eqs. (B4) and (B5).

$$f_{ret} = -\frac{\Delta G}{\Delta x} \approx -4x\gamma \quad \text{(B4)}$$

$$\Delta x \approx -\frac{4\gamma}{E} \quad \text{(B5)}$$

Inserting (B3) into (B5), we obtain Eq. (B6)

$$\Delta t \approx \frac{8\gamma}{E}\frac{t}{x} \quad \text{(B6)}$$

Assuming that there are n^* plates in the unit thickness in ND, we obtain the total deformation along ND, ΔL_{ND}, to be given by Eq. (B7)

$$\Delta L_{ND} = \Delta t n* \approx \frac{8\gamma}{E}\frac{t}{x}n* \quad \text{(B7)}$$

Hence, the contribution of the retraction to αl_{ND}, $\Delta L_{ND}/L_{ND}$, is given by Eq. (B8), corresponding to Eq. (16) in the text

$$\frac{\Delta L_{ND}}{L_{ND}} \approx \frac{n*}{L_{ND}}\frac{8\gamma}{E}\frac{t}{x} \quad \text{(B8)}$$

References

[1] Moore Jr EP. Polypropylene handbook. Münich: Carl Hanser Verlag; 1996.
[2] Brandrup J, Immergut EH. Polymer handbook. 3rd ed. New York: Wiley; 1989. p. V27–33.
[3] Landolt Bornstein Zahlenwerteund Funktionen aus Physik, Chemie, Astronomie, Geophysik und Technik 6 Aufl IIBand1 Teil. Berlin: Springer; 1971. p. S379–448.
[4] Kikuchi H, Koyama K. Polym Eng Sci 1996;36:1326.
[5] Nomura T. PhD Thesis, Nagoya University; 1994.
[6] Nomura T, Nishio T, Taniguchi H, Hirai I, Hisamura N. Kobunshi Ronbunshu 1994;51:505.
[7] Diez-Gutierrez S, Rodriguez MA, De Saja JA, Velasco JI. J Appl Polym Sci 2000;77:1275.
[8] Choy CL, Chen FC, Ong EL. Polymer 1979;20:1191.
[9] Choy CL, Chen FC, Young K. J Polym Sci, Polym Phys Ed 1981;19:335.
[10] Yamamori Y, Iwamoto K, Miwa Y. JSAE Rev 1991;12:61.
[11] Wu G, Nishida K, Takagi K, Sano H, Yui H. Polymer 2004;45:3085.
[12] Ono M, Washiyama J, Nakajima K, Nishi T. Polym J 2004;36:563.
[13] Rao N. Designing machines and dies for polymer processing with computer programs. Münich: Carl Hanser Verlag; 1981.
[14] Alexander LE. X-ray diffraction methods in polymer science. New York: Wiley; 1969.

[15] Capiati NJ, Porter RS. J Polym Sci, Polym Phys Ed 1977;15:1427.
[16] Wilchinsky ZW. J Appl Polym Sci 1963;7:923.
[17] Mondoza R, Regnier G, Seiler W, Lebrun JL. Polymer 2003;44:3363.
[18] Gu F, Hikosaka M, Toda A, Gosh SK, Yamazaki S, Arakaki A, et al. Polymer 2002;43:1473.
[19] Porter RS, Weeks NE, Capiati NJ, Krzewki RJ. J Therm Anal 1975;8: 547.
[20] Zollar P, Walsh DJ. Standard pressure–volume–temperature data for polymers. Lancaster, PA, USA: Technomic Publishing Co.; 1995.
[21] Raghara RS. Polym Compos 1988;9:1.
[22] Kerner EH. Proc Phys Soc 1956;B69:808.
[23] Holliday L, Robinson J. J Mater Sci 1973;8:301.
[24] Turner PS. J Res Nat Bur Stand 1946;37:239.
[25] Shapery RA. J Compos Mater 1968;2:380.
[26] Wang TT, Kwei TK. J Polym Sci, Part A-2 1969;7:889.
[27] Cribb JL. Nature 1968;220:576.
[28] Burkley CP, McCrum NG. J Mater Sci 1973;8:1123.
[29] Tashiro K, Kobayashi M, Tadokoro H. Polym Prepr Jpn 1986;35: 3266.
[30] The numerical factor, which would depend on the shape of the domain, is on the order of 1, indicating that the contribution from the retraction would be on the order of ~ 10 (10^{-5} m/m/°C). Hence, the contribution from the retraction will still be important.
[31] Gramespacher H, Messner J. J Rheol 1997;1:27.